INSTITUTE OF PHYSICS PUBLISHING PHYSICS IN MEDICINE AND BIOLOGY

Phys. Med. Biol. **49** (2004) 2197–2208 PII: S0031-9155(04)69915-5

3D tomographic reconstruction of coronary arteries using a precomputed 4D motion field

Christophe Blondel[1,2], Régis Vaillant[2], Grégoire Malandain[1] and Nicholas Ayache[1]

[1] INRIA, 2004 route des Lucioles, BP93, 06902 Sophia Antipolis Cedex, France
[2] General Electric Medical Systems, 283 rue de la Minière, 78530 Buc, France

E-mail: Christophe.Blondel@sophia.inria.fr, Regis.Vaillant@med.ge.com, Gregoire.Malandain@sophia.inria.fr and Nicholas.Ayache@sophia.inria.fr

Received 1 October 2003
Published 19 May 2004
Online at stacks.iop.org/PMB/49/2197
DOI: 10.1088/0031-9155/49/11/006

Abstract

In this paper, we present a new method to perform 3D tomographic reconstruction of coronary arteries from cone-beam rotational x-ray angiography acquisitions. We take advantage of the precomputation of the coronary artery motion, modelled as a parametric 4D motion field. Contrary to data gating or data triggering approaches, we homogeneously use all available frames, independently of the cardiac phase. In addition, we artificially subtract angiograms from their background structures. Our method significantly improves the reconstruction, by removing both motion and background artefacts. We have successfully tested it on the datasets from a synthetic phantom and 10 patients.

(Some figures in this article are in colour only in the electronic version)

1. Purpose

We present a new method to perform the 3D tomographic reconstruction of beating coronary arteries from one single run of a rotating monoplane cone-beam x-ray coronarography system.

Classical tomographic algorithms make the assumption that the object to be reconstructed remains still during acquisition. The 3D tomographic reconstruction of an object that is in motion during sinogram acquisition remains a challenging problem. This difficulty particularly applies to coronary artery reconstruction, for which two motions occur, namely breathing and heart beat. To address this issue, most of the proposed approaches rely on data gating or triggering, which indeed attempts to force the data compliance with respect to tomographic algorithm assumptions. A different way of addressing the problem is to incorporate a motion model in the reconstruction process. For instance, in CT acquisitions, some recent advances allowed one to deal with moderate amplitude motions as in Grangeat *et al* (2002).

In x-ray angiography imaging context, the 'CT-like' rotational acquisition mode has already been used to compute 3D reconstructions of static vascular structures such as intra-cranial or peripheral vessels (Anxionnat *et al* 2001). But, in the case of coronary arteries, cardiac contraction induces a high amplitude and high speed motion that make direct tomographic formulations irrelevant.

In Blondel *et al* (2003), we developed an algorithm to automatically determine a 4D parametric motion field of coronary arteries from one rotational x-ray sequence. In this paper, we present a *dynamic* tomographic algorithm that compensates for the coronary artery motion along the cardiac contraction, by taking advantage of 4D motion field precomputation. Contrary to previously proposed approaches, which used only a limited number of quasi-synchronous views as in Rasche *et al* (2002), our method uses homogeneously all available images, independently from the cardiac phase at which they were acquired.

The x-ray sequences are acquired on a digital flat panel coronarography system, with a rotational planar trajectory. This trajectory is defined by a cranial/caudal angle that is constantly 0° (0 rad) and a left/right anterior oblique angle amplitude ranging between 120° $\left(\frac{2\pi}{3}\,\text{rad}\right)$ and 200° $\left(\frac{10\pi}{9}\,\text{rad}\right)$. The maximum rotation speed of the gantry is 40° s^{-1} $\left(\frac{2\pi}{9}\,\text{rad}\,\text{s}^{-1}\right)$.

2. Methods

We first describe the two main prerequisites of our *dynamic* tomographic reconstruction method: artificial subtraction of background structures in angiograms and modelling of coronary artery motion. We then design a tomographic reconstruction method that compensates for object motion and derive a discrete resolution scheme. We finally describe a practical tomographic reconstruction algorithm, in the context of coronary artery motion and respiration.

2.1. Artificial subtraction

Contrary to intra-cranial or peripheral x-ray rotational angiography, a prior mask acquisition (without contrast agent injection) cannot be performed because physiological conditions of the acquisition, namely both respiratory and cardiac motions, cannot be exactly recovered, nor synchronized with the acquisition system rotation. Thus, no direct data subtraction can be done to produce images with removed background structures. However, we need to artificially subtract the angiograms from their background structures to prevent parasite structure backprojection during the reconstruction process. Producing subtracted images without corresponding masks is a difficult task. In Close *et al* (2002), the authors propose a subtraction method relying on layer decomposition of the angiograms. To achieve background subtraction, only layers containing the object of interest are retained.

We use a simpler method, based on already available information: a vessel detector. The artificial subtraction process is performed in two steps. First, a multiscale vessel detector, described in Sato *et al* (1998) and Krissian *et al* (2000), discriminates whether pixels belong to a vessel or not. This binary mask is then dilated to prevent vessel data loss. Second, a morphological closure operator is applied to the angiogram (Serra 1982) and used to compute an artificial background value. The dilated binary mask and the closure of the angiogram are then combined: if a pixel belongs to a vessel, according to the dilated binary mask, its artificial mask value is the corresponding value of the closure of the image, or else its artificial mask value is the same as the original image value. Finally, the logarithmic subtraction of

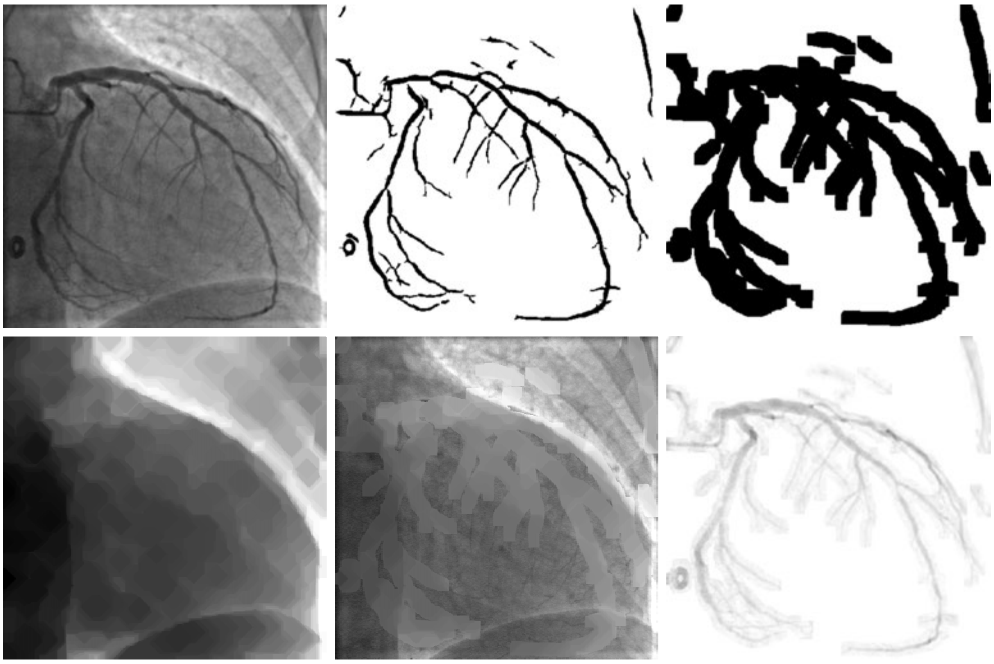

Figure 1. Top: (left) original angiogram with many visible background structures, (middle) result of binary vessel detection (mask) on the angiogram and (right) dilated binary mask. Bottom: (left) closure of the original angiogram, (middle) artificial mask angiogram and (right) artificially subtracted angiogram. Most of the background structures are removed in the subtracted angiogram.

the artificial mask from the original angiogram is performed to produce the actually used sinogram.

Figure 1 shows the effect of artificial subtraction on an angiogram from a patient dataset. In section 3, we will show comparative results that confirm the benefit of artificial subtraction.

2.2. 4D parametric motion

The key of the presented method is the incorporation of a precomputed 4D motion field in the tomographic reconstruction process. We briefly describe how we conduct this precomputation step.

The primary step is the 3D reconstruction of the coronary artery centrelines, which is performed in three phases. We first define a *reference time* in the cardiac cycle time. Usually, we choose end diastole as reference time because it corresponds to the most relaxed and most stable heart phase. We then select at least three quasi-synchronous angiograms acquired from different points of view, at this particular cardiac cycle time. Coronary artery centrelines in these angiograms are automatically segmented, using a multiscale vessel detector (Krissian *et al* 2000). Using stereovision, 3D points are reconstructed from the 2D segmentations. To improve the consistency of the 3D reconstruction, we developed a dedicated dynamic-programming-based matching algorithm (Blondel *et al* 2002). The 3D reconstruction process typically results in a 3D centreline model, consisting of 5000–20 000 points. At this point, it should be noted that the respiratory motion has not been corrected yet. This motion can be approximated by a 3D translation, mostly in the axial direction (Wang *et al* 1995). We compensate this motion by adapting the camera acquisition parameters

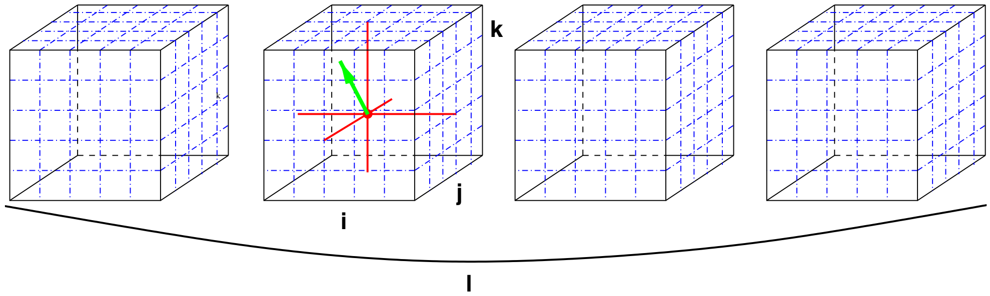

Figure 2. Schematic representation of a 4D B-solid. Indices i, j and k describe space coordinates and index l describes time coordinate. An example 3D parameter vector $\mathbf{p}_{ijkl}$ at one given control point is represented in green.

to make the projection images coherent with the 3D reconstruction. This is achieved by performing a bundle adjustment step (Triggs *et al* 2000). We iterate 3D reconstruction and bundle adjustment and end up with a stable 3D reconstruction and an estimation of the translation due to respiratory motion at the reference time frames. These translational corrections are finally used to estimate, using linear interpolation, the respiratory motion in the entire sequence. Consequently, the subsequent steps will no longer have to consider the respiratory motion effect.

We then compute the 4D motion of the coronary arteries from the 3D centreline model. We define a reference time in the cardiac cycle, arbitrarily set to 0 at which we want to perform the 3D reconstruction. This reference time can differ from the 3D reconstruction reference time, but, in practice, they are chosen to be equal.

Combining this reference time and cardiac periodicity we assign to every frame, indexed by n, a 'normalized ECG time' t_n between 0 and 1, representing the heart phase at which the frame was acquired. For instance, a normalized ECG time equal to 0 means that the cardiac phase was the reference time, while a normalized ECG time equal to 0.5 indicates that the cardiac phase was delayed by half a cardiac period from the reference time. In this way, we allow for cardiac period changes along the acquisition, but we assume that the heart motion remains spatially repeatable, which means that every spatial conformation is recovered at possibly varying time offsets.

We now compute a 4D parametric motion for the x-ray sequence. The parametrization we chose is a 4D B-solid (Radeva *et al* 1997). It is a 4D tensor product of B-splines, which is a smooth and semilocal representation, that makes it adapted to cardiac motion fitting. If we denote by $\{B_i\}_i, \{B_j\}_j, \{B_k\}_k$ the B-spline function bases along space coordinates, $\{B_l\}_l$ the B-spline function basis along time coordinate and $\mathbf{p}_{ijkl}$ the 3D vector at control point given by indices i, j, k, l, belonging to global parameter vector $\mathbf{p}$, then the position of point $X = (x, y, z)$ at time t in 4D B-solid motion is given by the relationship

$$\Phi(\mathbf{p}, X, t) = X + \sum_i B_i(x)\left(\sum_j B_j(y)\left(\sum_k B_k(z)\left(\sum_l B_l(t)\cdot \mathbf{p}_{ijkl}\right)\right)\right).$$

Figure 2 illustrates the representation of a given 3D vector $\mathbf{p}_{ijkl}$ at one control point. The vector $\mathbf{p} = \{\mathbf{p}_{ijkl}\}_{ijkl}$ is the parameter vector of the 4D B-solid.

The motion model is then fitted to a given specific dataset using a large scale optimization process. The optimal motion maximizes an energy function combining an external energy, evaluating the superimposition of projected deformed 3D centreline points with vessels in the angiograms and an internal regularizing energy, preventing degenerated motions (Blondel *et al* 2003). If we denote by $\mathcal{X}$ the set of points describing the 3D centreline model, $\mathcal{N}$ the set of images from which the motion is estimated, m_n the projection matrix associated with frame n, r_n the multiscale vessel detector associated with frame n and $\mathrm{Reg}_{\mathbb{R}^3\times\mathbb{R}}\Phi(\mathbf{p},\cdot,\cdot)$ a regularity measure, in space and time, on motion $\Phi(\mathbf{p},\cdot,\cdot)$, the criterion we optimize is

$$\Psi(\mathbf{p}) = \sum_{n\in\mathcal{N}}\sum_{X\in\mathcal{X}} r_n(m_n(\Phi(\mathbf{p}, X, t_n))) + \alpha\,\mathrm{Reg}_{\mathbb{R}^3\times\mathbb{R}}\Phi(\mathbf{p},\cdot,\cdot).$$

The 4D B-Solid motion model typically has 10 control points along each space coordinate and 10 control points along time coordinate. As the motion model is defined by a 3D vector at each control point, the parameter vector to be optimized is approximately of size 30 000. This large scale optimization problem is solved using a conjugate gradient algorithm (Gill *et al* 1982).

Let $\mathbf{p}^\star$ be the optimal parameter vector found by the optimization process. We denote as $\Phi : \mathbb{R}^3 \times \mathbb{R} \longmapsto \mathbb{R}^3$ the optimal 4D motion field $\Phi(\mathbf{p}^\star,\cdot,\cdot)$. $\Phi(X, t)$ gives the position, at time t, of the 3D physical point that was in position X at reference time. In particular, $\Phi(X, 0) = X$. Choosing t equal to a given t_n, for a given frame index n, $\Phi(\cdot, t_n)$ provides the new position after motion of any 3D point, and consequently its 2D projected position in the frame, as we have the projection matrix m_i associated with the frame.

2.3. Motion compensated 3D tomographic reconstruction

In the case of cardiac structures, motion correction is mandatory to achieve sharp reconstructions, without motion artefacts. In De Murcia (1996), the author proposes a method that iteratively extracts the radial component of the left ventrical motion from the projection set along the cardiac cycle and then improves the reconstruction by integrating motion knowledge. In contrast, as our motion estimation method is based on single-pass computer-vision algorithms, it does not require to be iterated between motion estimation and reconstruction. Additionally, both radial and tangential components of the motion are recovered, as the motion is estimated from 1D structures. As opposed to other proposed approaches in coronary angiography (Movassaghi *et al* 2003) that compensate for motion observed in the image plane with a tracking technique, our motion correction relies on a motion computed over 3D space and the entire cardiac cycle.

Taking advantage of the 4D precomputed motion field, we now design a *dynamic* tomographic algorithm.

The physical quantity we want to evaluate is the linear attenuation of the medium under observation. We allow for the 3D physical point motion along time, using the precomputed 4D motion field.

We now derive our formulation of the tomographic reconstruction of an object, whose sinogram is acquired for object motion. We denote by X any physical 3D point, t any acquisition time, 0 is considered as the reference time, at which we want to reconstruct the linear attenuation map. $\mu : \mathbb{R}^3 \times \mathbb{R} \longmapsto \mathbb{R}$ is the linear attenuation of any physical 3D point, varying along time, and $\Phi : \mathbb{R}^3 \times \mathbb{R} \longmapsto \mathbb{R}^3$ is the motion application representing the position at a given time of the physical 3D point that was in a given position at the reference time. For any given time t, $\Phi(\cdot, t)$ is denoted by Φ_t. We suppose that Φ_t is a diffeomorphism, for any time t. More specifically, the Jacobian in space coordinates of Φ_t is supposed to be such that $\det(\nabla\Phi_t(X)) > 0$, for any X. This physically means that two distinct physical 3D points cannot move to the same position. This hypothesis is physiologically true for cardiac motion, as myocardial material is not infinitely compressible.

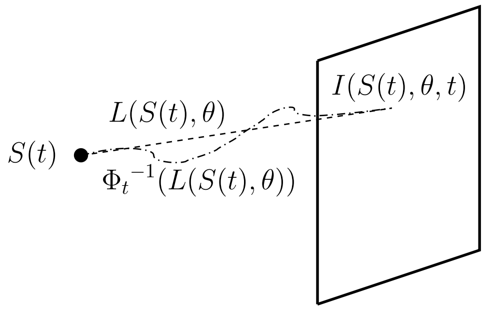

Figure 3. Effect of object motion incorporation in line integral computation: the line integral on $L(S(t), \theta)$ becomes a curve integral on $\Phi_t^{-1}(L(S(t), \theta))$.

We suppose that linear attenuation remains constant along acquisition time. This practically means that we neglect the contrast agent propagation and diffusion effects during the acquisition. Formally, it is equivalent to

$$\mu(\Phi_t(X), t) = \mu(\Phi_0(X), 0) = \mu(X, 0). \tag{1}$$

We now want to correlate the line integrals $I(X, \theta, t)$ of the linear attenuation $\mu(\cdot, t)$ along the line support $L(X, \theta)$ at any acquisition time t to the linear attenuation at the reference time $\mu(\cdot, 0)$

$$I(X, \theta, t) = \int_{L(X,\theta)} \mu(Y, t)\,\mathrm{d}Y$$

$$= \int_{\Phi_t^{-1}(L(X,\theta))} \mu(\Phi_t(Z), t).|\det(\nabla\Phi_t(Z))|\,\mathrm{d}Z \tag{2}$$

$$= \int_{\Phi_t^{-1}(L(X,\theta))} \mu(Z, 0).\det(\nabla\Phi_t(Z))\,\mathrm{d}Z. \tag{3}$$

Equation (2) is given by setting the variable substitution $Z = \Phi_t^{-1}(Y)$ in the integral. It is well defined, considering that Φ_t is a diffeomorphism. The second step, in equation (3), is deducted from our assumption on $\mu(\Phi_t(Z))$ constantness along time t (equation (1)) and from the positivity of $\det(\nabla\Phi_t(Z))$ (equation (2)).

We now consider the sinogram acquisition of an object in known motion as the sinogram acquisition of the same object considered still in its position at reference time. As shown in figure 3, the change induced by motion incorporation lies in the fact that line integrals have become curve integrals.

As show in figure 4, we integrate over angular sector Θ to define pixel value $P(S(t), \Theta, t)$ as a function of $\mu(\cdot, 0)$:

$$P(S(t), \Theta, t) = \int_{\Theta} I(S(t), \theta, t)\,\mathrm{d}\theta$$

$$= \int_{\Phi_t^{-1}(L(S(t),\Theta))} \mu(Z, 0).\det(\nabla\Phi_t(Z))\,\mathrm{d}Z.$$

We finally derive the practical discrete solving algorithm, corresponding to the former continuous problem formulation. The 3D space at reference time is discretized as voxel set $\{C_k\}_k$.

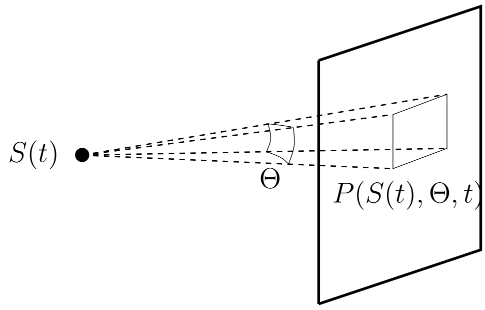

Figure 4. Illustration of pixel value $P(S(t), \Theta, t)$ formation.

Considering the voxel cube C in discretized 3D space at reference time, where $\mu(\cdot, 0)$ is now supposed to have a constant value denoted by $\mu(C)$, the contribution of voxel cube C to pixel value $P(S(t), \Theta, t)$ is given by

$$R(P(S(t), \Theta, t), C) = \int_{\Phi_t^{-1}(L(S(t),\Theta))\cap C} \mu(Z, 0).\det(\nabla\Phi_t(Z))\,\mathrm{d}Z$$

$$= \mu(C) \int_{\Phi_t^{-1}(L(S(t),\Theta))\cap C} \det(\nabla\Phi_t(Z))\,\mathrm{d}Z \tag{4}$$

$$= \mu(C) \int_{\Phi_t(\Phi_t^{-1}(L(S(t),\Theta))\cap C)} \det\left(\nabla\Phi_t\left(\Phi_t^{-1}(Y)\right)\right).\det\left(\nabla\Phi_t^{-1}(Y)\right)\mathrm{d}Y \tag{5}$$

$$= \mu(C) \int_{L(S(t),\Theta)\cap\Phi_t(C)} \det\left(\nabla\Phi_t\left(\Phi_t^{-1}(Y)\right)\right).\det\left(\nabla\Phi_t^{-1}(Y)\right)\mathrm{d}Y \tag{6}$$

$$= \mu(C) \int_{L(S(t),\Theta)\cap\Phi_t(C)} \mathrm{d}Y \tag{7}$$

$$= \mu(C)\cdot\mathrm{vol}(L(S(t), \Theta)\cap\Phi_t(C)). \tag{8}$$

Equation (4) is deducted from $\mu(\cdot, 0)$ constantness over C. The variable substitution $Y = (Z, t)$ leads to equation (5). The injectivity of Φ_t induces equation (6). Finally, equation (7) is given by a property of the Jacobian matrix of a reciprocal function: $\det(\nabla f^{-1}(f(a))) = \frac{1}{\det(\nabla f(a))}$.

As the computed contribution is linear with respect to $\mu(\cdot, 0)$ (equation (8)), as in the static case, we can denote by R^{Φ} the matrix associated with the projection operator in motion. $\mu(\cdot, 0)$ is denoted μ, and the discrete subtracted sinogram data (pixels) are denoted $\mathbf{d}$. The discrete problem to be solved can be stated as

$$R^{\Phi}\cdot\mu = \mathbf{d}.$$

Using index notation, let the coefficient $R^{\Phi}_{j_i,k}$ in matrix R^{Φ} be the contribution of the voxel k to the pixel value j_i, belonging to frame i. We denote by S_{j_i} the solid angle with vertices the corners of pixel j_i and the x-ray source position $S(t_i)$. In the dynamic case, using equation (8), we take the motion field into account by replacing the voxel cube C_k by its image under the 3D motion field Φ_{t_i}:

$$R^{\Phi}_{j_i,k} = \mathrm{vol}\left(S_{j_i}\cap\Phi_{t_i}(C_k)\right).$$

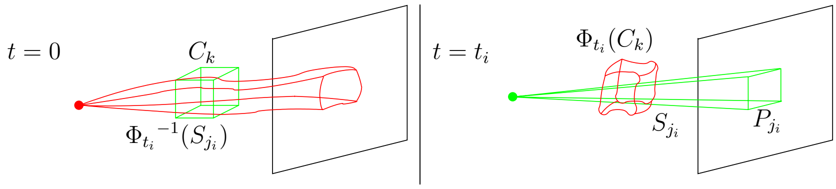

Figure 5. The contribution of voxel C_k considered at time $t = 0$ to pixel P_{j_i} considered at time $t = t_i$ can be related to (left) the intersection between S_{j_i} and $\Phi_{t_i}(C_k)$ at time $t = t_i$, or to (right) the intersection between $\Phi_{t_i}^{-1}(S_{j_i})$ and C_k at time $t = 0$.

Figure 5 summarizes the relations between voxels at reference time $t = 0$ and pixels at frame times $t = t_i$.

As mentioned in the continuous formulation, the projection operator matrix now depends on the motion field Φ. In addition, we remark that setting Φ to identity application I leads to the classical static formulation of voxels to pixels contribution:

$$R^I_{j_i,k} = \mathrm{vol}\big(S_{j_i} \cap C_k\big).$$

In practice, $S_{j_i} \cap \Phi_{t_i}(C_k)$ cannot be easily estimated, we thus decide to use single contribution matrices: a voxel is supposed to contribute to one single pixel. Indeed, the motion of the voxel cubes is reduced to the motion of their centres. Let c_k be the centre of the voxel cube C_k, we have:

$$R^\Phi_{j_i,k} = \begin{cases} \mathrm{vol}\big(\Phi_{t_i}(C_k)\big) & \text{if } \Phi_{t_i}(c_k) \in S_{j_i} \\ 0 & \text{else.} \end{cases}$$

The evaluation of quantity $\mathrm{vol}\big(\Phi_{t_i}(C_k)\big)$ is still very expensive. But, we know that variation between $\mathrm{vol}\big(\Phi_{t_i}(C_k)\big)$ and $\mathrm{vol}(C_k)$ is bounded by $\det\big(\nabla\Phi_{t_i}\big)$ extremal values. We evaluated these bounds experimentally for some precomputed motion fields, with end diastole selected as reference time. On patient datasets, we observed that this volume variation is 0.92 in average and bounded by 0.80 and 1.04. To reduce the computational cost of our algorithm, we decided to neglect the volume variation effect, which allows us to set

$$R^\Phi_{j_i,k} = \begin{cases} \mathrm{vol}(C_k) & \text{if } \Phi_{t_i}(c_k) \in S_{j_i} \\ 0 & \text{else.} \end{cases}$$

If we denote by m_i the projection matrix associated with frame i, then the former statement becomes the practical scheme we use:

$$R^\Phi_{j_i,k} = \begin{cases} \mathrm{vol}(C_k) & \text{if } m_i\big(\Phi_{t_i}(c_k)\big) \in P_{j_i} \\ 0 & \text{else.} \end{cases}$$

It is important to remark that, as the motion only impacts the projection operator matrix computation, the former description is general enough to make it appropriate for all classes of tomographic algorithms. In our context, we have chosen to use the additive ART technique (Herman 1980) because of its efficiency and robustness for vascular structure 3D reconstruction.

3. Results

First, we tried our method on a synthetic phantom, consisting of tubular structures of various diameters, animated under a homothetic motion, coarsely modelling myocardium contraction. We compared the results obtained with the classical static ART algorithm and with the motion

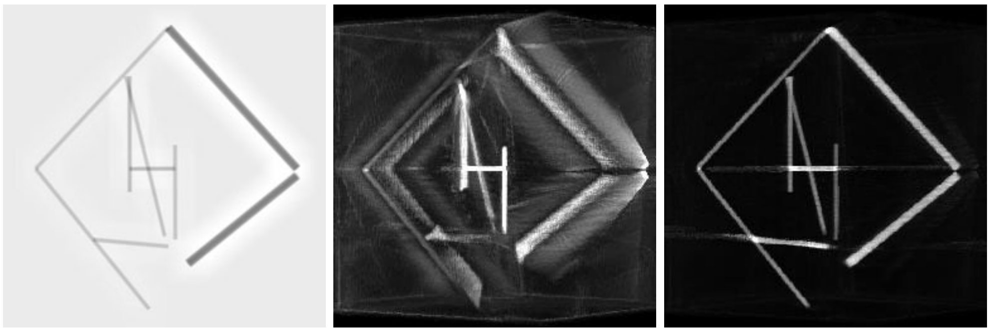

Figure 6. (Left) original attenuation image of the beating phantom (with vessels in dark), (middle) maximum intensity projection view of the 3D reconstruction without motion compensation and (right) maximum intensity projection view of the 3D reconstruction with motion compensation (with high attenuations in bright). We notice that structures coplanar to the acquisition plane present some light reconstruction artefacts.

compensated ART algorithm. The results showed that the blur induced by the object motion is removed by taking into account the precomputed motion, as illustrated in figure 6. Only some light artefacts remain for tubular structures that are coplanar to the acquisition plane. This demonstrates that our formulation is able to address the motion problem in this acquisition context.

Then, we applied our *dynamic* 3D tomographic reconstruction algorithm to 10 patient datasets. These sequences typically consist of 100 angiograms, with 17 cm field-of-view width, providing a $120^\circ \left(\frac{2\pi}{3}\text{ rad}\right)$ angular range. The separate and combined effects of artificial subtraction and motion compensation are shown in figure 7.

To assess the 3D reconstructions for the patient datasets, we compared their projection to static sequences acquired on the same patient but with angles not belonging to the initial rotational trajectory. This comparison is shown in figure 8.

As illustrated in figure 9, we also computed projections at mechanically non-reachable angles and thus provide virtual views that cannot be acquired in practice.

From the clinical point of view, 3D reconstructions provide relevant extra information compared to original angiogram sequences. For instance, up to third order vessels can be visualized from any 3D point of view, and stenoses (narrowed parts of vessels that induce myocardial infarct risks) can be quantified in terms of lumen 2D absolute surface measure (see figure 10), instead of 1D projected diameter measures, which depend greatly on the frame's point of view.

Comparing the 3D reconstruction results obtained with the different patient datasets, we characterized two key factors for the reconstruction quality:

- the angular coverage has to be at least $120^\circ \left(\frac{2\pi}{3}\text{ rad}\right)$ to prevent from obtaining anisotropic reconstructions,
- the 4D motion field has to be accurate to obtain sharp 3D reconstructions: every defect in the precomputed motion field induces blur in the neighbourhood of voxels having inaccurate motion information.

We implemented our method in C++ under Linux, and parallelized it using PVM (Geist *et al* 1993). When run on four clustered Xeon at 2 GHz biprocessor workstations, the typical preprocessing time for the 4D motion computation is 30 min and the typical 3D reconstruction time is 40 min to complete a 256^3 voxel reconstruction from 100 angiograms,

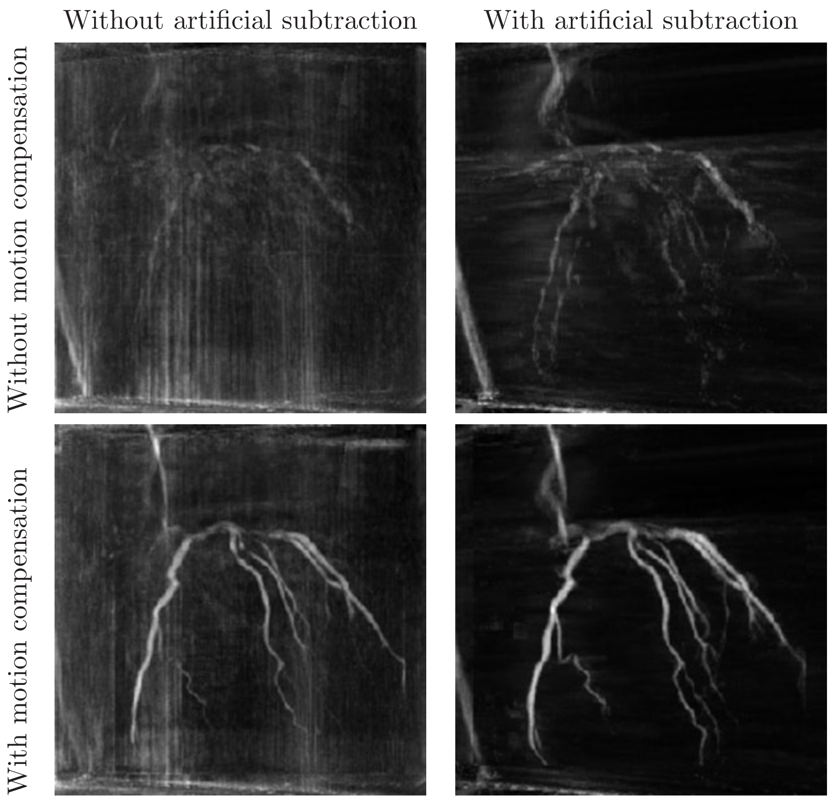

Figure 7. Orthographic maximum intensity projection views in sagittal direction of different 3D reconstructions from the same x-ray sequence, showing the separate and combined effects of artificial subtraction and motion compensation on the tomographic reconstruction of coronary arteries.

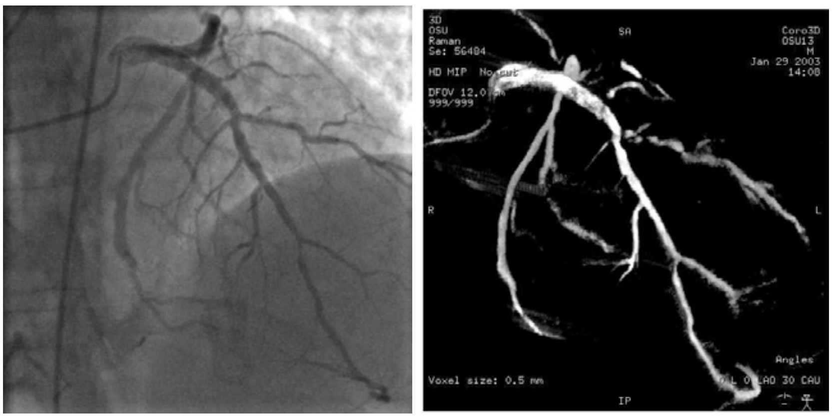

Figure 8. (Left) angiogram acquired at left/right anterior oblique angle 0° (0 rad) and Cranial/Caudal angle −30° ($-\frac{\pi}{6}$ rad), not belonging to the dataset used for reconstruction, to be compared to (right) the projection of the 3D reconstruction under the same acquisition system angles.

Figure 9. From left to right: coronal, sagittal and axial orthographic maximum intensity projection views of a patient dataset 3D reconstruction—axial view is mechanically infeasible on a vascular gantry. In this case, it provides a nice visualization of the left main artery of the patient, with a curious double lumen.

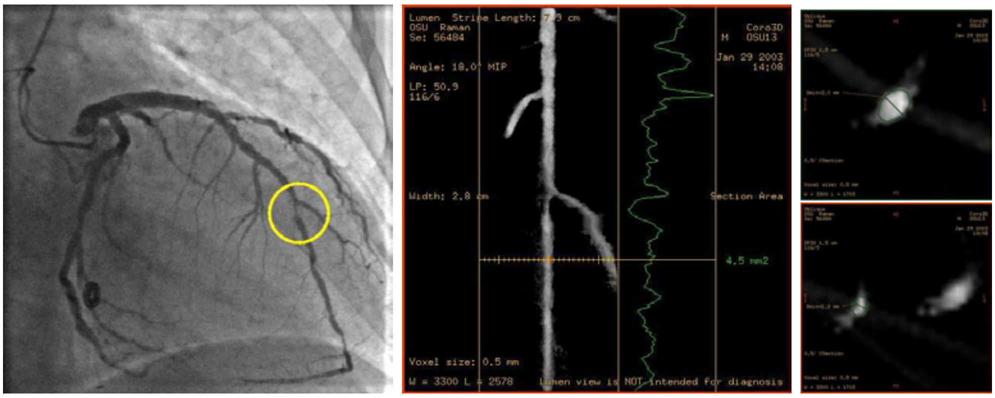

Figure 10. From left to right: 2D localization of a stenosis of interest, unfolded vessel description from the 3D reconstruction, including its mean diameter, its section and its curvilinear abscissa, and (top) a sectional view of the proximal part of the vessel to be compared to (bottom) a sectional view of the stenotic part of the vessel.

involving two iterations of the additive ART algorithm. During the 3D tomographic reconstruction process, most of the computational cost is dedicated to the evaluation of the voxel motion.

4. Conclusion

We presented a new method to compute 3D tomographic reconstructions of coronary arteries moving under cardiac contraction, which utilizes the entire angiogram sequence, by taking into account a precomputed 4D motion field. The 3D tomographic reconstructions of coronary arteries are drastically improved by motion compensation and artificial subtraction.

The motion-compensated 3D tomographic reconstruction results should allow for anatomical 3D measurements of clinical interest such as vessel and lesion length, vessel and lesion 3D diameter and transversal section surface. This will be the subject of a more extensive validation process.

Our future aims are to compute more accurately the coefficients of the projection operator matrix (by taking into account the local compression/dilatation effect and using non-single contributions) and to test our approach with other classical tomographic methods. Another interesting perspective of this work is its potential combination with saddle trajectories (Pack *et al* 2003) that would prevent reconstruction artefacts for the vessels that are coplanar to the acquisition plane.

Acknowledgments

The authors thank Dr Raman, Dr Magorien and Dr Bush at Ohio State University, Columbus, USA and Dr Rüdiger Simon at Universtaetsklinikum, Kiel, Germany for acquiring and providing them with patient rotational sequences.

References

Anxionnat R, Bracard S, Ducrocq X, Trousset Y, Launay L, Kerrien E, Braun M, Vaillant R, Scomazzoni F, Lebedinsky A and Picard L 2001 Intracranial aneurysms: clinical value of 3D digital subtraction angiography in the therapeutic decision and endovascular treatment *Radiology* **218** 799–808

Blondel C, Malandain G, Vaillant R and Ayache N 2003 4D deformation field of coronary arteries from monoplane rotational x-ray angiography *Proc. Computer Assisted Radiology and Surgery 2003* vol 1256 of ICS (London: Elsevier) pp 1073–8

Blondel C, Vaillant R, Devernay F, Malandain G and Ayache N 2002 Automatic trinocular 3d reconstruction of coronary artery centerlines from rotational x-ray angiography *Computer Assisted Radiology and Surgery 2002 Proc.* (Paris: Springer) pp 832–7

Close R, Abbey C and Whiting J 2002 Improved localization of coronary stents using layer decomposition *Comput. Aided Surg.* **7** 84–9

De Murcia J 1996 Reconstruction d'images cardiaques en tomographie d'émission monophotonique à l'aide de modèles spatio-temporels *PhD Thesis* Institut National Polytechnique de Grenoble

Geist A, Beguelin A, Dongarra J, Jiang W, Manchek R and Sunderam V 1993 PVM 3 user's guide and reference manual *Technical Report* ORNL/TM-12187, Oak Ridge National Laboratory

Gill P, Murray W and Wright M 1982 *Practical Optimization* (New York: Academic)

Grangeat P, Koenig A, Rodet T and Bonnet S 2002 Theoretical framework for a dynamic cone-beam reconstruction algorithm based on a dynamic particle model *Phys. Med. Biol.* **47** 2611–25

Herman G 1980 *Image Reconstruction from Projections* (New York: Academic)

Krissian K, Malandain G, Ayache N, Vaillant R and Trousset Y 2000 Model-based detection of tubular structures in 3D images *Comput. Vis. Image Underst.* **80** 130–71

Movassaghi B, Rasche V, Viergever M, Niessen W and Florent R 2003 3D coronary reconstruction from calibrated motion-compensated 2D projections *Proc. Computer Assisted Radiology and Surgery 2003* vol 1256 of ICS (London: Elsevier) pp 1079–84

Pack J, Noo F and Kudo H 2003 Investigation of a saddle trajectory for cardiac CT imaging in cone beam geometry *Proc. 7th Int. Conf. on Fully 3D Reconstruction and Nuclear Medicine* ed Y Bizais *(Saint-Malo)*

Radeva P, Amini A and Huang J 1997 Deformable b-solids and implicit snakes for 3D localization and tracking of spamm mri data *Int. J. Comput. Vis. Image Underst.* **66** 163–78

Rasche V, Grass M, Koppe R, Bücker A, Günther R, Kühl H, Op de Beek J, Bertrams R and Suurmond R 2002 ECG-gated 3D rotational coronary angiography *Proc. Computer Assisted Radiology and Surgery 2002* (Paris: Springer) 826–31

Sato Y, Nakajima S, Shiraga N, Atsumi H, Toshida S, Koller T, Gerig G and Kikinis R 1998 3D multi-scale line filter for segmentation and vizualisation of curvilinear structures in medical images *Med. Image Analysis* **2** 143–68

Serra J 1982 *Image Analysis and Mathematical Morphology* (New York: Academic)

Triggs B, McLauchlan P, Hartley R and Fitzgibbon A 2000 Bundle adjustment—A modern synthesis *Vision Algorithms: Theory and Practice* vol 1883 of LNCS ed W Triggs, A Zisserman and R Szeliski (Berlin: Springer) pp 298–375

Wang Y, Riedere S and Ehman R 1995 Respiratory motion of the heart: kinematics and the implications for the spatial resolution in coronary imaging *Magn. Reson. Med.* **33** 713–9